

# Design and Implementation of an Inexpensive LIDAR Scanning System with Applications in Archaeology

Andrew Willis<sup>a</sup>, Yunfeng Sui<sup>a</sup>, William Ringle<sup>b</sup>, Katherina Galor<sup>c</sup>

<sup>a</sup>UNC - Charlotte, 9201 University City Blvd., Charlotte, NC 28223

<sup>b</sup>Davidson College, Davidson, NC 28035

<sup>c</sup>Brown University, Providence, RI 02912

## ABSTRACT

*This paper describes the development of a system and associated software capable of capturing 3D LIDAR data from surfaces up to 20m from the sensor. The chief concern of this initial system is to minimize cost which, for this initial system, is approximately \$10.5k (USD). Secondary considerations for the system include portability, robustness, and size. The system hardware consists of two motors and a single-point sensor, capable of measuring the range of a single surface point location. The motors redirect the emitted laser along lines nearly equivalent to that specified by a spherical coordinate system generating a spherical range image,  $r = f(\phi, \theta)$ . This article describes the technical aspects of the scanner design which include a bill-of-materials for the scanner components and the mathematical model for the measured 3D point data. The designed system was built in 2007 and has since been used in the field twice: (1) for scanning ruins and underground cisterns within Mayan cities near Merida, Mexico and (2) for scanning the ruins of a Crusader castle at Apollonia-Arsuf, located on the Mediterranean shore near Herzliya, Israel. Using this system in these vastly different environments has provided a number of useful insights or “best practices” on the use of inexpensive LIDAR sensors which are discussed in this paper. We also discuss a measurement model for the generated data and an efficient and easy-to-implement algorithm for polygonizing the measured 3D  $(x, y, z)$  data. Specific applications of the developed system to archaeological and anthropological problems are discussed.*

## 1. INTRODUCTION

Light Distance And Ranging (LIDAR) sensors have been in used for research in the geosciences and astronomical contexts for many years to recover range measurements of surfaces very far from the measuring system. NASA's Clementine probe launched in 1994 carried a LIDAR system capable of measuring geometry from 640km away. Applications of this technology at much shorter ranges has become widespread in many disciplines. Examples of current applications include the detection of forest structures to track the spatial distribution of some tree species [1, 2], detecting road surface damage [3], and detecting man-made structures from regular patterns in aerial LIDAR data [4].

As the price of this technology becomes more affordable, new applications for these sensors are being explored in a wide variety of disciplines. This article focuses on the design, implementation, and deployment of a newly developed LIDAR scanning prototype system for use in the field by archaeologists and anthropologists.

Traditional methods for measurement in archaeological contexts make use of theodolites or similar surveying equipment to map terrain [5]. While these methods are very useful for measuring key points at sites, there are several benefits associated with capturing a very large amount of 3D data using a 3D LIDAR capture system. Most benefits associated with LIDAR in this context are based the ability of LIDAR sensors to capture accurate data quickly that characterizes the detailed scene geometry in terms of a surface mesh consisting of typically 100k - 5M 3D point measurements [6].

Unfortunately, current LIDAR sensing systems are still too costly, sensitive, and heavy for the vast majority of archaeologists. Consequently, when such equipment is necessary, specialists are hired or the equipment is rented for a short period of time to capture specific geometric areas of interest. The developed system is a step towards making this technology more affordable and usable for cultural heritage researchers.

---

Further author information: (Send correspondence to A. Willis)

A. Willis: E-mail: arwillis@uncc.edu, Telephone: 1 704 687 8420

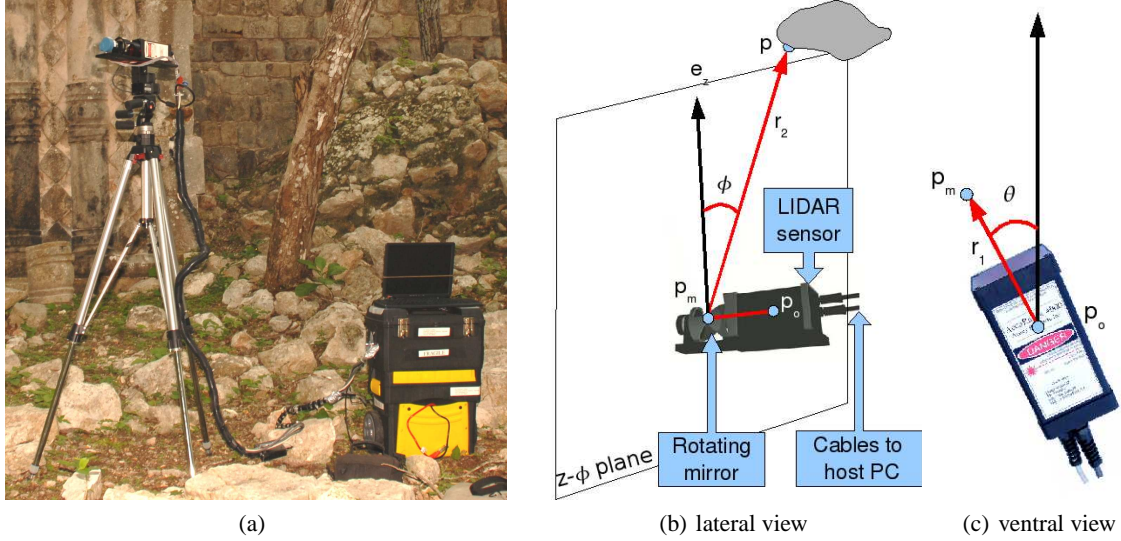


**Figure 1.** Parameters of the measurement model include three Euclidean positions: (1)  $\mathbf{p}_o$ , the coordinate system origin and the location where the laser return is sensed, (2) the location where the laser is reflected off the rotating mirror,  $\mathbf{p}_m$ , and (3) the location of the sensed data point  $\mathbf{p}$ . Orientation parameters include the angle,  $\phi$ , of the mirror with respect to the global coordinate system  $z$ -axis,  $\mathbf{e}_z$ , and the rotational position of the scanning head  $\theta$ . (a) is a view of the described scanning system in operation at the Kuic site in the vicinity of Oxcutzcab, Mexico (June 2007). (b) shows a lateral (side) view of the scanning head for a fixed horizontal angle  $\theta$ . (c) shows a ventral (top) view of the scanning head and shows the horizontal (pan) angle,  $\theta$ , controlled by a pan motor that varies the longitudinal position.

LIDAR scanning is now a commonplace within the cultural heritage community [7–10]. Current efforts seek to develop automated systems that integrate scan data to form global site models [4, 11], urban models [12], or improve the overall texture and geometry model appearance [9]. This article focuses on the more pragmatic problem of developing low-cost LIDAR systems that can be used in remote contexts where navigating robots for automated LIDAR may be impractical. These are often locations of new and exciting cultural heritage finds that cannot be moved (ruins/caves/tombs) while also being endangered either by the threat of looting or by the potential for collapse due to structural deterioration. In such cases, new tools such as that described in this article are of critical importance.

## 2. MEASUREMENT MODEL

We start with a simplistic model of the data generation process which defines a spherical world coordinate system whose origin is the location of the LIDAR sensor. The scene is then modeled as a spherical range image  $r = f(\phi, \theta)$  with respect to this point where  $r$  is the radius of a scene surface at colatitude or zenith angle  $\phi$  and azimuthal angle  $\theta$  on the unit sphere. For each  $(\phi, \theta)$  position on the unit sphere, the sensor emits a pulse of infra-red laser that either (i) reflects off a scene surface generating a range measurement or (ii) there is no measurement generated. In situation (i) we assume that the range measurement is due to a direct reflection from a surface in the scene, i.e., we do not account for several possible optical phenomenon such as surface inter-reflections, refraction, or translucence. Situation (ii) may occur due to numerous reasons such as absorption of the radiation (“dark” surfaces), no reflection (sky/out-of-range surfaces), or insufficient energy reflected back to the sensor (specular/translucent surfaces).

In construction of the sensor, we begin with a single-point range sensor capable of measuring radius in only one direction which we assign to angles  $(\phi = 0, \theta = 0)$ . The single-point sensor is converted to a line-scanner by mounting a rotating mirror oriented at a  $45^\circ$  angle with respect to the direction of the emitted LIDAR signal. The mirror is rotated by a motor whose position is recorded by an optical encoder. Since the mirror reflects the emitted laser along a  $90^\circ$  angle, rotation of the mirror allows for range measurements to be taken that fall along all latitudes for a single line of longitude on the sphere. Different latitude values are represented by the variable  $\phi \in [0, 2\pi)$  on the unit sphere. The collection of components consisting of the mirror, encoder, motor and single-point LIDAR sensor are mounted along a common rail and are collectively referred to as the “sensing head.” The sensing head is then mounted onto a pan motor which varies the azimuthal angle of the sensor,  $\theta \in [0, \pi)$  (see Figure 1).

$$\mathbf{R}(\phi, v_x, v_y, v_z) = \begin{bmatrix} \cos \phi + v_x^2(1 - \cos \phi) & v_x v_y(1 - \cos \phi) - v_z \sin \phi & v_x v_z(1 - \cos \phi) + v_y \sin \phi \\ v_x v_y(1 - \cos \phi) + v_z \sin \phi & \cos \phi + v_y^2(1 - \cos \phi) & v_y v_z(1 - \cos \phi) - v_x \sin \phi \\ v_x v_z(1 - \cos \phi) - v_y \sin \phi & v_y v_z(1 - \cos \phi) + v_x \sin \phi & \cos \phi + v_z^2(1 - \cos \phi) \end{bmatrix}$$

**Figure 2.** The Euclidean matrix that operates on  $(x, y, z)$  points. The operation is equivalent to a counter-clockwise rotation about the unit vector  $\mathbf{v} = (v_x, v_y, v_z)^t$ .

Our initial spherical measurement model must be modified to take into consideration the mechanical construction of the system. These constraints include:

1. Addition of a rotating mirror and associated motor and motor position encoder to measure the mirror position.
2. Addition of a pan motor which rotates the sensing head, i.e., the sensor and mirror assembly, horizontally.
3. Mounting of the unit offsets the sensor from the origin.

which include an offset of the origin due to inaccuracies in mounting the 3D sensor.

Denote the 3D scene point being measured as  $\mathbf{p} = (x, y, z)^t$ , the point where the mirror reflects the outgoing and incoming infra-red laser as  $\mathbf{p}_m$ , and the sensor location as the world coordinate system origin,  $\mathbf{p}_o$ . Without loss of generality, we assume that the sensor location,  $\mathbf{p}_o$ , is located exactly at the origin,  $\mathbf{p}_o = (0, 0, 0)^t$  and that the vector  $\mathbf{p}_m - \mathbf{p}_o$  lies in the  $xy$ -plane, i.e.,  $\mathbf{p}_m = (x_m, y_m, 0)^t$ .

We now want to define a mapping from Euclidean space to the spherical coordinate system within which we are measuring the data points. We start by stating the equation of the measured range data point in terms of the defined variables.

$$r = \|\mathbf{p} - \mathbf{p}_m\| + \|\mathbf{p}_m - \mathbf{p}_o\|$$

The overall range measurement is then divided into two parts  $r_1$  and  $r_2$  such that  $r_1 = \|\mathbf{p}_m - \mathbf{p}_o\|$  and  $r_2 = \|\mathbf{p} - \mathbf{p}_m\|$ , then  $r = r_1 + r_2$ . Note that  $r_1$  is a fixed distance determined by the bracket upon which both the LIDAR sensor and the rotating mirror are mounted. For our application, this distance is 43.69mm (1.72in). We then describe the vector  $\mathbf{p} - \mathbf{p}_m$  in terms of a vector in the direction of the Euclidean coordinate system  $z$ -axis,  $\mathbf{e}_z = (0, 0, 1)^t$ , rotated by an angle  $\phi$  about the unit vector  $\mathbf{p}_m - \mathbf{p}_o$ . The vector  $\mathbf{p}_m - \mathbf{p}_o$  is a vector that describes the orientation of the scanning head in the  $xy$ -plane and is a polar coordinate system vector, i.e.,  $\mathbf{p}_m - \mathbf{p}_o = (r_1 \sin \theta, r_1 \cos \theta, 0)^t$ . Using the Rodriguez formula, the general Euclidean rotation matrix describing rotation about the vector  $\mathbf{v} = (v_x, v_y, v_z)^t$  by an angle of  $\phi$  is given in Figure (2). We can then write down the measured 3D point  $\mathbf{p} = (x, y, z)^t$  as a function of the measured variables as follows:

$$\mathbf{p} = r_1 \mathbf{p}_m + (r - r_1) \mathbf{R}(\phi, \sin \theta, \cos \theta, 0) \mathbf{e}_z \quad (1)$$

Since the values of both  $\mathbf{e}_z$  and  $\frac{\mathbf{p}_m - \mathbf{p}_o}{\|\mathbf{p}_m - \mathbf{p}_o\|}$  are known, we can simplify the equation (1) above.

$$\begin{bmatrix} x \\ y \\ z \end{bmatrix} = \begin{bmatrix} r_1 \cos \theta + (r - r_1) \cos \theta \sin \phi \\ r_1 \sin \theta - (r - r_1) \sin \theta \sin \phi \\ (r - r_1) \cos \phi \end{bmatrix} \quad (2)$$

If either  $\mathbf{p}_m$  or  $\mathbf{e}_z$  change, the equation for  $\mathbf{p}$  may become significantly more complicated potentially involving up to twenty four additional terms. Hence the coordinate system selected produces 3D  $(x, y, z)$  point measurements that are a relatively simple function of the measured variables.

An optical encoder mounted to the back of the rotating mirror motor provides 4096 distinct latitude positions for  $\phi \in [0, 2\pi)$ . Pan motor positions are discretized into 14000 distinct position for  $\theta = [0, \pi)$ . However, as the measured data is ordered, more dense samplings are possible via interpolation. With this in mind, the sampling period in  $\phi$  is determined by the angular velocity of the mirror motor. The sampling period in  $\theta$  is determined by the angular velocity of the pan motor. Both of these parameters are user-defined via the LIDAR measurement system software.

Description	Cost
Bogen Manfrotto Tripod (B&H Photo)	\$327.90
Tripod Carrying Case (B&H Photo)	\$124.95
Shuttle Mini Computer Shuttle SD32G2B (Black) Intel Socket 775 SFF Barebone Intel Core 2 Duo E6320 1.86GHz / 4MB Cache / 1066MHz FSB / Conroe / Dual-Core / OEM / Socket 775 / Processor Megavision MV141 / 14" / XGA 1024 x 768 / VGA / Black / LCD Monitor (Tigerdirect.com)	\$800.00
Directed Perception PTU-D46-70 Pan-Tilt Unit	\$2100.00
Acuity Laser Measurement AR4000 LIDAR Sensor	\$3495.00
Acuity Laser Measurement Rotating Mirror / Encoder Assembly	\$2295.00
Acuity Laser Measurement PCI High Speed Interface Card (50k samples/sec)	\$1495.00
(Optional) Acuity Laser Measurement PCI High Speed Interface Card (200k samples/sec)	\$2495.00
Total (using the 50k PCI card)	\$10458.00

**Table 1.** A bill of materials list for the components that combine to form the proposed scanning system.

As with all LIDAR sensors, the time-of-flight for the transmitted and received infra-red laser pulse is measured and converted to a distance. Uncertainties in the measured distance are associated with uncertainties in the detection of the arrival time of the reflected laser pulse. Under the appropriate conditions, the sensor can resolve this time accurately enough to guarantee ranges to within 2.5mm. However, the accuracy of measurements depends on the sampling rate and at a rate of 50kHz the error increases to approximately 5mm.

The major consideration for the design of this system was to minimize cost. For this reason, we integrated a line-scanner sensor from Acuity Research (AR4000) with a pan-tilt unit from Directed Perception. The sensing hardware was mounted to a Manfrotto tripod and controlled by a mini-computer for processing the data in real-time. The bill-of-materials for these items are provided in Table (1) and the total cost of the as-built system was approximately ~\$11k (USD).

### 3. POLYGONIZING MEASUREMENTS

Measurements from the sensor are ordered in both  $\phi$  and  $\theta$ , hence, a trivial polygonization scheme may be implemented that connects sequential samples along constant values for each parameter to generate a quadrangular mesh. Yet, as mentioned previously, some samples may not be recorded for specific locations that do not reflect enough energy to generate a measurement. Additionally, we often wish to extract a mesh with lower resolution than that present in the raw scan data. For this reason we implement a simple “balloon” style polygonization scheme similar to that from [13]. Our estimate is a three-step process as follows:

1. For our balloon model, we initialize the surface by defining a set of equi-distant points along the surface of the unit sphere. The number of points is user-controlled and determines the number of polygons in the resulting polygonization of the measured data.
2. The measured data is then projected onto the unit sphere and each point is associated with sample closest to it on the spherical surface. Closest neighbors are computed trivially from the dual-mesh of the user-defined tessellation that defines intervals of  $(\phi, \theta)$  around each spherical surface sample.
3. We then estimate the 3D surface position by minimizing the sum of squared differences between each sampled spherical surface points and those measured points associated with each surface point. Those spherical surface points with no associated measurement data are deleted from the mesh and correspond to holes on the estimated surface.

This algorithm is very simple to implement and the minimization has a simple explicit solution. Hence, the surface estimates are quickly computed from the measured data at a user-defined resolution. Results of this interpolation are shown in Figures (3b,d) and (4b,d).

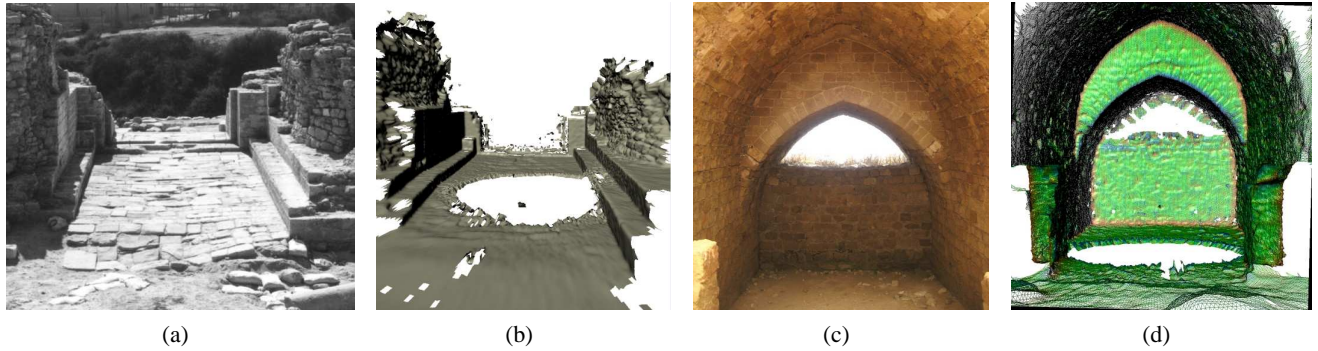


**Figure 3.** (a,c) show digital images of the gate, (a), and the donjon, (c), of the Crusader fortress at Apollonia-Arsuf. (b,d) show views of the 3D scans of the same locations from a similar vantage point. (d) has been colorized to highlight geometric details via a local estimate of mean curvature at each measured surface location using [14].

## 4. RESULTS

The developed LIDAR system was used in two different localities during the summer of 2007: (i) Oxcutzcab, Mexico on the Yucatan Peninsula and (ii) Apollonia-Arsuf site on the Mediterranean shore near Herzliya, Israel. Scanning within Mexico focused on scanning houses, ceremonial structures, and underground cisterns (known as *chultuns*) at three different sites: Huntichmul, Kuic, and Labna. Scanning within Israel focused on scanning ruins of the front gate and drawbridge of a Crusader fortress.

### 4.1. The Crusader Fortress at Apollonia-Arsuf

The Crusaders captured Apollonia-Arsuf, or Arsur as it was called from now on, in 1101 A.D. They restored the existing fortifications and added new ones. In the northern part of the city they erected a castle, destroyed in 1265 A.D. by the Mamluk sultan Baybars, and left in ruins ever since. Large scale excavations of the castle were undertaken in 1998, 1999 and 2000 exposing the remaining components of the structure's latest phase. These include: 1) a central irregular courtyard; 2) the main pentagonal fortification complex, with a gate on the east flanked by two semi-circular towers with an additional semi-circular tower, as well as a donjon and two square corner towers in the west; 3) an external fortification wall; 4) a moat with outer retaining wall; 5) a series of vaulted halls and retaining walls along the cliff at the western facade of the fortress; 6) and finally a small harbor.

During the summer of 2007 the authors Willis, Sui and Galor conducted an experimental survey of the castle focusing on the eastern gate, the drawbridge in the southeast, and various architectural elements from the collapsed structure scattered around the site, in particular on the beach to the west and the moat to the east and south of the fortification. Among other tools the team used a LIDAR Scanning System to capture architectural features with the highest possible accuracy. Though the castle has been previously photographed and measured, the only 3D renderings of the site drawn by artists are highly conjectural. Those drawings are partially based on plans and sections, routine sketches made during the course of the excavation. The major difficulty in providing an accurate representation of the entire castle lies in the fact that for most parts only the foundations and lower wall sections of the castle are preserved. To match the scattered architectural fragments manually or physically with the *in situ* remainder of the fortification is impossible.

Only few projects in Israel have used automated 3D-scanning for capturing archaeological materials. Noteworthy among those are attempted reassemblies of pottery vessels at Dor [15] and the documentation of a funerary structure outside of Jerusalem [10]. Unfortunately, however, most archaeologists working in Israel view those tools as esoteric, redundant and excessively expensive. Yet, the desire to recreate a highly accurate representation of an object, structure or site as a whole, is one of the most basic and essential goals of the archaeologist. The more visually precise, the better are we able to recreate the past.

There was very little protection from the elements at the Apollonia-Arsuf site and the period during which scans were taken in July 2007 was a very hot period with temperatures commonly in the vicinity of 30°C. The strength of the sun in this case reduced the accuracy of the scanned surfaces significantly. The scan data noise introduced by the effect of direct sunlight appears to be additive and non-stationary. Current work seeks to characterize this noise process to improve the quality of scan data under strong sunlight conditions.

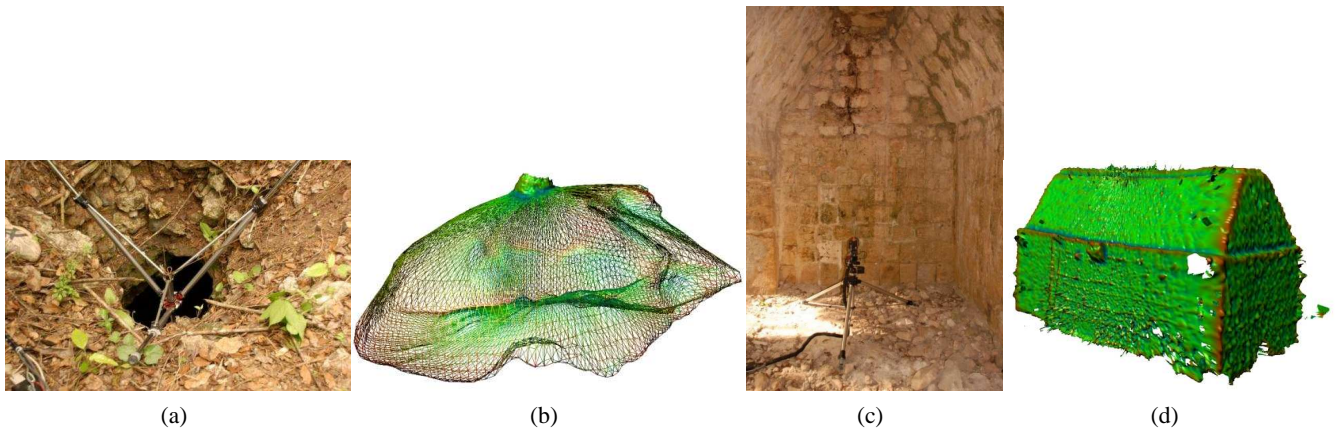


**Figure 4.** (a,c) show digital images of the scanning system measuring a *chultun*, (a), and a dwelling, (c), within the Mayan settlement at Huntichmul. (b,d) show scan results for the chultun (~24k polygons) and dwelling (~380k polygons) respectively. (c) is shown in wire frame to reveal details of the internal geometry of the cistern. Both (c,d) have been colorized to highlight geometric details as in Figure (3d).

#### 4.2. Mayan Cisterns and Buildings at Huntichmul, Kuic, and Labna

Although imaging techniques such as multispectral scanning has been used with success in Mesoamerica for decades, 3D laser scanning technology is only now being applied. To our knowledge, the only applications to date involve the recording of small portable objects and sculpture [16–18]. Application of the technology to immovable archaeological features and architecture will permit their registration far more quickly and accurately than by conventional methods.

Initial experiments with the LIDAR sensor were conducted during late June, 2007, at the Maya archaeological site of Huntichmul, Yucatan, Mexico, under investigation since 2004 by Ringle as one facet of the Labna-Kiuc Archaeological Project. Huntichmul lies within the Puuc subregion, a hilly area famous for its ancient reliance upon water storage technology. Presently it is completely forested and difficult of access. Despite substantial rainfall, surface water is almost completely absent from this region due to the porous limestone substrate, so that inhabitants were forced to laboriously excavate cisterns (*chultuns*) into the soft marl below the caprock, then seal the chambers with stucco. These *chultuns* were often quite capacious, with a roughly beaker-shaped chamber 3m and more in depth, and a narrow neck only 50-100 cm in diameter.

Since *chultuns* were the only source of water during the dry season, they have been used to model past population levels using estimates of daily per capita water consumption [19]. However, the narrow neck and depth of the chambers prevents easy inspection of their interiors, and most recent work still quotes *chultun* measurements made at a single site many years ago [20]. It is clear, however, that *chultuns* vary greatly in size and are often irregular in shape, making estimates of their volume difficult. Entering *chultuns* to measure them is not desirable because, in addition to being uncomfortable and occasionally dangerous, it is preferable to leave deposits within the chambers undisturbed, as they sometimes contain useful artifacts and ecofacts that need to be excavated with care.

Use of the LIDAR scanner opened the possibility of imaging the interiors of *chultuns* with minimal intrusion. Lowering the inverted scanning head permitted recording of the interior in a matter of minutes. The narrow neck limited the amount of ambient light, so scans recorded relatively little noise. Usually only a small cone directly above the sensor head could not be scanned.

A detailed record of *chultun* size will allow us to investigate are the correlation between chamber size, placement criteria, and social factors. Does capacity correlate with the number of rooms on a given platform? Does it instead correlate with social status? Did larger capacity *chultuns* favor certain physical settings (e.g., on- or off-platform, in upland or valley floor settings), perhaps related to the ease of excavation into the bedrock. Do we see chronological trends in *chultun* development? Since one hypothesis for the rapid abandonment of the Puuc heartland c. A.D. 900 is an extended drought, were large capacity *chultuns* developed late in the sites' histories?

The second application tested the ability of the instrument to record the interior and exterior facades of several standing masonry buildings at Huntichmul and two neighboring Puuc sites, Kiuic and Labna. The distinctive Puuc architectural style flourished between A.D. 650-900 [21] and is characterized by extensive friezes of decorative stonework composed of colonnettes, geometric motifs, and elaborate composite masks of Maya deities. Measurement and drawing of such structures is laborious and costly by conventional methods, and facades are often idealized to save time. LIDAR scanning in contrast potentially offered rapid, highly detailed, and geometrically accurate representations of buildings in their current states. Such images could be used to monitor building deterioration, to make virtual comparisons between buildings, and to model structural stresses. In cases where large sections of a building have fallen intact, scans could be used to create a virtual reconstruction.

LIDAR's limited range required several scans per facade, plus at least one per room interior. Multiple scans also helped account for occlusions, though it became apparent that some sort of vertical elevation of the sensor would be necessary to fully register projecting upper cornices and moldings. Multiple scans also required adequate overlaps between sections, particularly the entryways linking rooms with exterior facades, and the development of an accurate method of splicing raw images.

The scanner generally performed as anticipated despite hot, humid field conditions. Although portable, the scanner was bulky with the main portability limitation being the car battery powering the system. At this site we also observed significant errors when attempting to scan under direct sunlight which remains an area of investigation for improvement.

## 5. CONCLUSIONS

This paper has detailed a new prototype system that seeks to address a critical need for practical use of LIDAR sensors in field archaeology and anthropology. The system is based on a short-range LIDAR sensor which captures 3D  $(x, y, z)$  surface points at a typical distances of 5-10m and, under ideal conditions, can capture data from surfaces up to 15m from the sensor. A mathematical model for data generation is discussed and a simple technique for polygonizing the data is demonstrated. Trials of the prototype system show promising results with successful data-collection efforts in remote areas of the Yucatan peninsula on Mayan dwellings and cisterns and in Israel on the ruins of a Crusader fortress gate and drawbridge. The prototype system is proof-of-concept that inexpensive LIDAR sensors can be used under the difficult conditions of field archaeology and anthropology, even in remote locations. There are no systems available with similar capabilities at a comparable cost of approximately ~\$11k (USD). While the initial tests show promise, many shortcomings still exist for the system. Future systems would be less bulky, have low power requirements, require less calibration, and have sensors that produce data at a farther range that is robust to ambient light (sunlight) and variations in surface reflectivity, i.e., dark or specular surfaces.

## REFERENCES

1. N. Skowronski, K. Clark, R. Nelson, J. Hom, and M. Patterson, "Remotely sensed measurements of forest structure and fuel loads in the pinelands of new jersey," *Remote Sensing of Environment* **108**, pp. 123-129, 2007.
2. J. B. Drake, R. O. Dubayah, D. B. Clark, R. G. Knox, J. B. Blair, M. A. Hofton, R. L. Chazdon, J. F. Weishampel, and S. D. Prince, "Estimation of tropical forest structural characteristics using large-footprint lidar," *Remote Sensing of Environment* **79**, pp. 205-319, 2002.
3. W. S. Wijesoma, K. R. S. Kodagoda, and A. P. Balasuriya, "Road-boundary detection and tracking using lidar sensing," *IEEE Transactions on robotics and automation* **20**, pp. 456-464, June 2004.
4. M. Doneus, C. Briese, M. Fera, and M. Janner, "Archaeological prospection of forested areas using full-waveform airborne laser scanning," *Archaeological Science* **35**, pp. 882-893, 2008.
5. W. Stone and G. Cheok, "Ladar sensing applications for construction," tech. rep., National Institute of Standards and Technology, 2001.
6. M. Hebert and E. Krotkov, "3d measurements from imaging laser radars: How good are they?," in *IEEE/RSJ international workshop on Intelligent Robots and Systems*, pp. 359-364, IROS, IEEE, (Osaka, Japan), Nov.3-5 1991.
7. R. Scopigno, P. Pingi, C. Rocchini, P. Cignoni, and C. Montani, "3d scanning and rendering cultural heritage artifacts on a low budget," in *European Workshop on "High Performance Graphics Systems and Applications"*, (Cineca, Bologna, Italy), Oct. 16-17 2000.
8. R. Scopigno, "3d scanning: Improving completeness, processing speed and visualization," in *Vision Modeling and Visualization*, p. 355, 2004.

9. P. K. Allen, I. Stamos, A. Troccoli, B. Smith, M. Leordeanu, and S. Murray, "New methods for digital modeling of historic sites," *IEEE Computer Graphics and Applications*, pp. 32–41, Nov. 2003.
10. J. Taylor, J. A. Beraldin, G. Godin, L. Cournoyer, M. Rioux, and J. Domey, "Nrc 3d imaging technology for museums and heritage," in *Proceedings of the First International Workshop on 3D Virtual Heritage*, pp. 70–75, October 2002.
11. P. S. Blaer and P. K. Allen, "Two stage view planning for large-scale site modeling," in *Intl. Symposium on 3D Data Processing, Visualization and Transmission*, June 2006.
12. F. Rottensteiner, "Automatic generation of high-quality building models from lidar data," tech. rep., IEEE Computer Society, 2003.
13. L. Cohen, "On Active Contour Models and Balloons," *Computer Vision, Graphics and Image Processing : Image Understanding* **53**(2), pp. 211–218, 1991.
14. H. Pottman and K. Opitz, "Curvature analysis and visualization for functions defined on euclidean spaces or surfaces," *Computer Aided Geometric Design* **11**, pp. 655–674, 1994.
15. H. Mara and R. Sablatnig, "3d-vision applied in archaeology," *Forum Archaeologiae - Zeitschrift für klassische Archäologie* **34**(3), 2005.
16. A. Powell, *Scanning History, Yaxchilan, Mexico*, Harvard University Gazette Online, 2007.
17. T. Doering and L. Collins, "The kaminaljuyú sculpture project: An expandable three-dimensional database," tech. rep., Report submitted to the Foundation for Mesoamerican Studies, Inc., Crystal River, FL, 2007.
18. T. Doering and L. Collins, "Mesoamerican three-dimensional imaging project," tech. rep., Report submitted to the Foundation for Mesoamerican Studies, Inc., Crystal River, FL, 2007.
19. P. McAnany, *In Precolumbian Population History in the Maya Lowlands*, ch. Water Storage in the Puuc Region of the Northern Maya Lowlands: A Key to Population Estimates and Architectural Variability, pp. 263–284. University of New Mexico Press, Albuquerque, 1990.
20. E. H. Thompson, *Memoirs of the Peabody Museum of American Archaeology and Ethnology*, vol. 1, ch. The Chultunes of Labna, Yucatan. Harvard University, Cambridge, 1897.
21. H. E. D. Pollock, *The Puuc. Memoirs of the Peabody Museum*, Peabody Museum of Archaeology and Ethnology, Harvard University, Cambridge, 1980.